From Orbit to Touchdown: A Comparative Study of Powered Descent Guidance Laws

Benjamin W. Salak[1]
The University of Alabama, Tuscaloosa, Alabama, 35487 USA

This paper demonstrates a common 3DOF dynamic simulation architecture to analyze the performance of different entry, descent, and landing (EDL) guidance architectures for a notional lunar landing probe. The guidance architectures examined are proportional and derivative (PD) control, zero effort miss and zero effort velocity (ZEM/ZEV I) control with a basic kinematic time to go estimator, and a zero effort miss and zero effort velocity (ZEM/ZEV II) control using the time-to-go estimation function from D'Souza guidance. The ZEM/ZEV II had the best accuracy; however, it took longer to land than ZEM/ZEV I. Both ZEM/ZEV models were consistent and regularly demonstrated better than expected nominal performance across a Monte Carlo simulation of orbit and burn initial conditions. The PD control was significantly more variable in performance and less accurate than the ZEM/ZEV cases. Across the Monte Carlo simulation the average miss distances were 1189 m, 0.00003894 m, and 0.000000004622 m. The average impact speeds were 14.58 m/s, 1.331 m/s, and 1.331 m/s. The average flight times were 1112 s, 862.0 s, and 1045 s. With a starting mass of 1000 kg and a dry mass of 300 kg, the final average vehicle masses were 315.2 kg, 401.6 kg, and 369.1 kg. Results are reported for PD, ZEM/ZEV I, and ZEM/ZEV II respectively.

I. Nomenclature

$\boldsymbol{r}_{\overline{x}}$	=	position vector in perifocal frame
h	=	orbital angular momentum
μ	=	gravitational parameter
e	=	orbital eccentricity
θ	=	orbital true anomaly
$\boldsymbol{v}_{\overline{x}}$	=	velocity vector in perifocal frame
$\boldsymbol{Q}_{X\overline{x}}$	=	direction cosine matrix of transformation from XYZ to $\overline{xyz}$
$\boldsymbol{r}_X$	=	position vector in body-centered inertial (BCI) frame
$\boldsymbol{v}_X$	=	velocity vector in BCI frame
m	=	mass of vehicle
$\boldsymbol{T}_X$	=	thrust force vector of vehicle in BCI frame
r_X	=	magnitude of position vector in BCI frame
$\ddot{\boldsymbol{r}}_X, \boldsymbol{a}_X$	=	acceleration vector in BCI frame
$\boldsymbol{a}_{gravity}$	=	gravity acceleration vector in BCI frame
$\boldsymbol{a}_{thrust}$	=	thrust acceleration vector in BCI frame
T_X	=	magnitude of thrust force vector in BCI frame
I_{sp}	=	specific impulse of vehicle engine
g_o	=	magnitude of Earth gravity
$\dot{m}$	=	mass flow rate
$v_{initial}$	=	initial orbital velocity
r_a	=	orbital radius at apoapsis

[1] Graduate Student, Aerospace and Engineering Mechanics, AIAA Young Professional.

a_{final} = final (desired) semi major axis
v_{final} = final (desired) orbital velocity
r_{final} = final (desired) orbital radius
t_{burn} = deorbit burn duration
Δv = change in velocity
v_X = magnitude of velocity vector in BCI frame
$\boldsymbol{a}_{X,cmd}$ = commanded acceleration vector in BCI frame
K_P = proportional gain constant
$\boldsymbol{e}_{position}$ = position error vector
K_D = derivative gain constant
$\boldsymbol{r}_{X,target}$ = target descent position vector in BCI frame
$\boldsymbol{e}_{velocity}$ = velocity error vector
$\boldsymbol{v}_{X,descent}$ = target descent velocity vector in BCI frame
v_{target} = target descent speed
a_{max} = maximum vehicle acceleration value
$a_{X,cmd}$ = magnitude of commanded acceleration vector in BCI frame
t_{go} = descent time-to-go value
$\boldsymbol{ZEM}$ = zero effort miss vector
$\boldsymbol{ZEV}$ = zero effort velocity vector
$\boldsymbol{g}_X$ = gravity vector in BCI frame
$r_{X,toTarget}$ = magnitude of distance to target point vector in BCI frame
$\boldsymbol{r}_{X,target}$ = distance to target point vector in BCI frame
a = D'Souza guidance coefficient "a"
b = D'Souza guidance coefficient "b"
c = D'Souza guidance coefficient "c"
Γ = D'Souza weighting coefficient "Γ"
g_X = magnitude of gravity vector in BCI frame

II. Introduction

This paper reviews the accuracy and propellant consumption of guided descent trajectories starting from a notional lunar orbit. A 3DOF simulation is configured with x, y, and z translation as the degrees of freedom (DOF). The simulation is designed to compare a proportional and derivative (PD) controlled descent, a zero effort miss (ZEM) and zero effort velocity (ZEV) controlled descent, and a second ZEM/ZEV descent using the polynomial time-to-go estimate derived in D'Souza guidance. A notional descent vehicle that has immediate thrust response and can thrust in any direction is used. The mass and engine specifications are based on recent lunar landers like JAXA's Smart Lander for Investigating the Moon (SLIM). SLIM weighed approximately 715 kg at launch and 200 kg at landing [1], meaning the lander's mass was approximately 72% propellant. This simulation uses 700 kg of propellant and 300 kg of dry mass for a clear percentage breakdown. The Intuitive Machines Nova-C lander used a VR900 engine producing 900 lbf or 4000 N of thrust [2]. This simulation sets the max thrust to 3000 N with an ISP of 300 s. Although the guidance methods simulated in this paper are simple compared to the terrain relative navigation and hazard avoidance employed on several recent Mars and Lunar missions, the foundational math is still relevant as Blue Ghost's M1 mission used D'Souza guidance during its EDL sequence from 20 km to 500 m in altitude [3]. For reference, SLIM was within 10 m of its target point at 50 m in altitude before the hazard avoidance sequence took control authority and piloted it to a safe landing site [1]. Blue Ghost M1 landed within its 100 m error ellipse [4].

III. 3DOF Simulation Architecture

The simulation initially uses Kepler-based equations to propagate the initial orbital conditions and then transitions to an ODE45-based solver for the dynamic EDL portion. This design was chosen as the initial orbit is easiest to propagate without the ODE45 solver, and ODE45 does not necessarily conserve energy, whereas the Kepler-based equations provide the correct orbital propagations. The Kepler equations are taken from equations in *Orbital Mechanics for Engineering Students* by Howard Curtis [5]. The initial orbit is simulated using the initial conditions provided by the user. The simulation uses an inertial fixed coordinate system centered on the target body. The initial orbit can be defined in three dimensions with the orbital elements. The orbital elements are angular momentum h,

eccentricity e, inclination i, right ascension of the ascending node (RAAN) Ω, argument of perigee ω, and true anomaly θ [5]. First, the position and velocity vectors can be computed in the perifocal frame as shown in Eqs. (1) and (2). The perifocal frame is a frame centered at the focus of the orbit, where the x-y plane is in the plane of the orbit, and the x direction vector is from the focus of the orbit to the periapsis [5].

$$\boldsymbol{r}_{\bar{x}} = \frac{h^2}{\mu}\frac{1}{1 + e \cdot \cos\theta} \cdot \begin{Bmatrix} \cos\theta \\ \sin\theta \\ 0 \end{Bmatrix} \tag{1}$$

$$\boldsymbol{v}_{\bar{x}} = \frac{\mu}{h} \cdot \begin{Bmatrix} -\sin\theta \\ e + \cos\theta \\ 0 \end{Bmatrix} \tag{2}$$

Next, the transformation matrix must be calculated to compute the transformation between the perifocal frame and the body-centered inertial frame. The origin is still at the orbit focus, but the x-y plane is in line with the body's equatorial plane. The matrices that are multiplied are shown in Eq. (3):

$$\boldsymbol{Q}_{X\bar{x}} = \begin{bmatrix} \cos\omega & \sin\omega & 0 \\ -\sin\omega & \cos\omega & 0 \\ 0 & 0 & 1 \end{bmatrix} \begin{bmatrix} 1 & 0 & 0 \\ 0 & \cos i & \sin i \\ 0 & -\sin i & \cos i \end{bmatrix} \begin{bmatrix} \cos\Omega & \sin\Omega & 0 \\ -\sin\Omega & \cos\Omega & 0 \\ 0 & 0 & 1 \end{bmatrix} \tag{3}$$

Next the body-centered inertial position and velocities vectors are computed in Eqs. (4) and (5):

$$\boldsymbol{r}_X = \boldsymbol{Q}_{X\bar{x}} \cdot \boldsymbol{r}_{\bar{x}} \tag{4}$$

$$\boldsymbol{v}_X = \boldsymbol{Q}_{X\bar{x}} \cdot \boldsymbol{v}_{\bar{x}} \tag{5}$$

With these equations, the initial velocities and positions are known to initiate descent. The ODE45 solver requires a state vector, shown in Eq. (6).

$$state = [\boldsymbol{r}_X \, \boldsymbol{v}_X \, m] \tag{6}$$

The state is composed of seven parameters: three to define the initial position in three degrees, three to define the velocity in three degrees, and one to define the mass of the vehicle. The ODE45 solver relies on a dynamics function to compute the updates to the state function. The core dynamic equation is provided below; all functions related to commanded thrust are discussed in the relevant guidance sections. Equation (7) is the equation driving the vehicle's dynamic response [5]:

$$\ddot{\boldsymbol{r}}_X = -\mu\frac{\boldsymbol{r}_X}{{r_X}^3} + \frac{\boldsymbol{T}_X}{m} \tag{7}$$

Equation (7) can be rewritten with the variables used in the dynamics function shown in Eq. (8):

$$\boldsymbol{a}_X = \boldsymbol{a}_{gravity} + \boldsymbol{a}_{thrust} \tag{8}$$

The last component of the state vector that requires updating is the vehicle mass term. Equation (9) gives the time rate of change of the mass, or mass flow rate, based on the rocket equation [5]:

$$\dot{m} = -\frac{T_X}{I_{sp} \cdot g_o} \tag{9}$$

The matrix shown in Eq. (10) is returned at the end of the dynamics function as the updated state vector:

$$state = [\boldsymbol{v}_X \, \boldsymbol{a}_X \, \dot{m}] \tag{10}$$

IV. Simulation Validation: Simple Deorbit Maneuver

To test the general working order of this simulation, a simple burn is programmed to reduce the velocity enough to cause an impact with the target body surface. This simulation validation scenario also tests the event termination and terminal statistics portions of the simulator. To estimate the timing of the burn, Kepler-based equations defined by Curtis [5] can be used. Effectively, the procedure is to reduce the periapsis, or lowest point of the orbit, to intersect with the surface, while executing the burn at the apoapsis. Equations (11–14) give the periapsis-lowering burn time:

$$v_{initial} = \frac{h}{r_a} \tag{11}$$

$$v_{final} = \sqrt{\frac{2 \cdot \mu}{r_a} - \frac{\mu}{a_{final}}} \tag{12}$$

$$a_{final} = r_a + r_{final\ (surface\ altitude)} \tag{13}$$

$$t_{burn} = \frac{\Delta v}{acceleration} = \frac{v_{final} - v_{initial}}{\frac{T_X}{m}} \tag{14}$$

Table 1 lists the notional values used to specify a simulation scenario.

Table 1 Parameters for deorbit simulation

Parameter Name	Parameter Value
Mass [kg]	1000
Max thrust [N]	3000
ISP [s]	300
[x0 y0 z0] [m]	[-2237000 0 0]
[vx0 vy0 xz0] [m/s]	[0 -1386 0]
Burn time [s]	0.75

As a result of the initial small burn, the vehicle deorbits, impacting 3947 s after the burn, approximately halfway through the orbit, as expected. Figures 1 through 3 show the performance of the deorbit burn. Figure 3 is an acceleration plot showing that, after the burn, the magnitude of the acceleration vector returns to the magnitude of lunar gravity, validating the basic simulation environment performance and the event termination system.

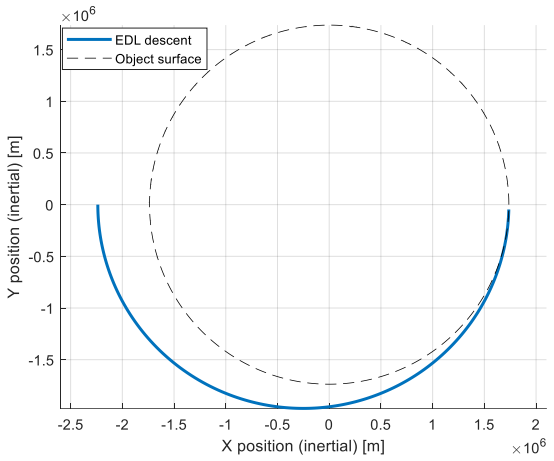

Fig. 1 **Deorbit bird's eye view.**

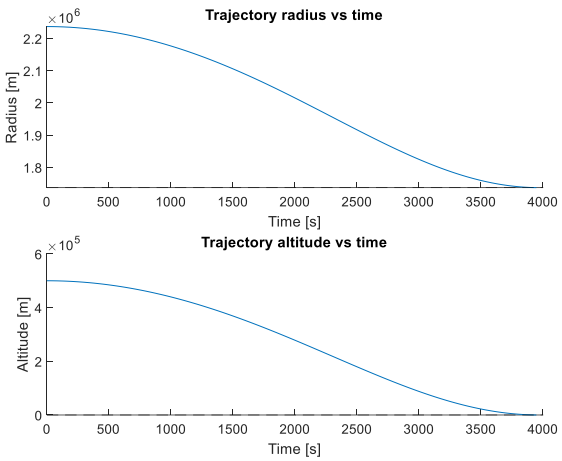

Fig. 2 Deorbit radius and altitude descent.

Although difficult to illustrate with a bird's eye view, Fig. 1 shows the EDL deorbit sequence starting at apoapsis on the left and slowing descending until the vehicle, its trajectory denoted by the blue line, impacts the object surface nearly 180 deg away from the burn as expected from Kepler's equations.

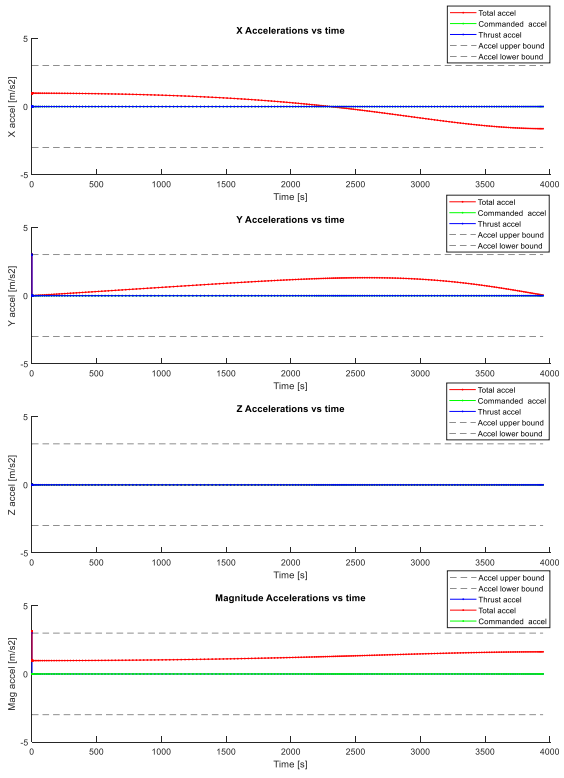

Fig. 3 Deorbit accelerations.

The burn is primarily seen as Y acceleration and, due to the time scale, only shows up as a small blip at the start. The burn is directed along the velocity vector using Eq. (15) [5]:

$$\boldsymbol{a}_{thrust} = \frac{T_X}{m} \cdot \frac{\boldsymbol{v}_X}{v_X} \tag{15}$$

V. Guidance Simulation: PD Control

The PD landing control is implemented after a rough burn period that decreases the horizontal (orbital) velocity and positions the vehicle closer to the target, which is roughly 13 deg ahead of the vehicle when the descent begins. The timeline of events is shown in Table 2.

Table 2 EDL sequence

Event	Parameter
Main deorbit burn	450 s
True anomaly at start of main deorbit burn	305 deg
Enabling of PD guidance	450 s after first event start
Target descent velocity	0.1 m/s
Descent cutoff altitude	0.5 m
Target angle on surface from periapsis	318 deg

The PD guidance uses Eqs. (16–19), and the gains are defined in Table 3. $\boldsymbol{v}_{X,descent}$ is defined to reduce the chance of the guidance commanding a prolonged hover before landing. The target descent velocity vector is set in the direction from the target on the surface to the current vehicle position. Additionally, in the pursuit of reducing the chance of hovering, all thrust is cut at 0.5 m to enable the simulated vehicle to free fall to the surface. The 0.5 m cutoff is programmed into all guidance modes.

$$\boldsymbol{a}_{X,cmd} = -K_P \cdot \boldsymbol{e}_{position} - K_D \cdot \boldsymbol{e}_{velocity} \tag{16}$$

$$\boldsymbol{e}_{position} = \boldsymbol{r}_X - \boldsymbol{r}_{X,target} \tag{17}$$

$$\boldsymbol{e}_{velocity} = \boldsymbol{v}_X - \boldsymbol{v}_{X,descent} \tag{18}$$

$$\boldsymbol{v}_{X,descent} = v_{X,target} \cdot \frac{\boldsymbol{r}_X - \boldsymbol{r}_{X,target}}{r_X - r_{X,target}} \tag{19}$$

Table 3 PD control gains

Gain Parameter	Gain Value
K_P	1
K_D	80

Because a PD controller is designed to adjust the transient response, while a PI controller focuses on the steady state error [6], a PD controller was used here. The definition of the PD controller is shown in Eq. (16), which functions by feeding the computed error, multiplied by the proportional gain, and the derivative of the error, multiplied by the derivative gain, forward to produce commanded accelerations [6]. In this scenario, the error is the position difference, and the derivative of the error is the velocity difference.

The logic shown in Eq. (20) is designed to force the commanded acceleration down to the engine's max allowable acceleration:

$$\boldsymbol{a}_{thrust} = a_{max} \cdot \frac{\boldsymbol{a}_{cmd}}{a_{cmd}} \tag{20}$$

The result is a descent shown in Figs. 4 through 9.

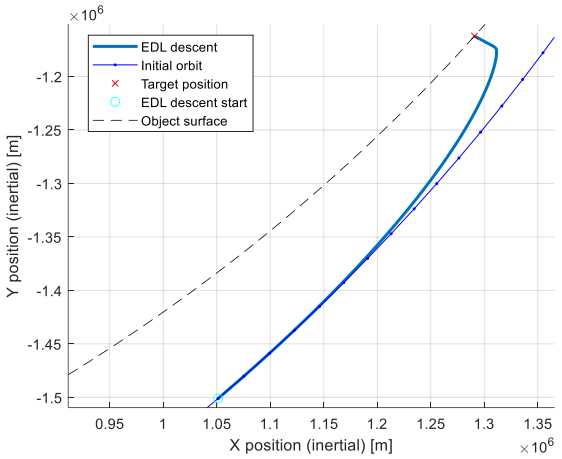

Fig. 4 PD EDL descent trajectory.

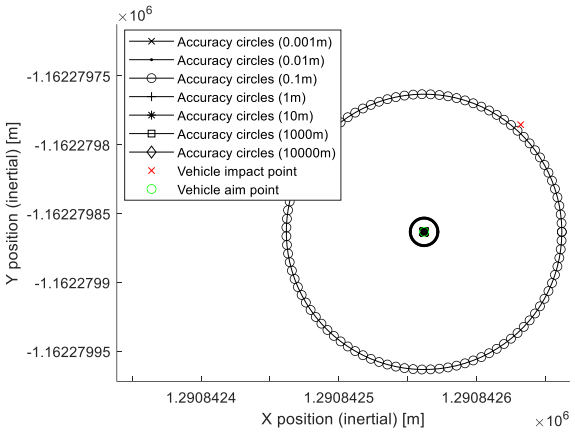

Fig. 5 PD landing accuracy.

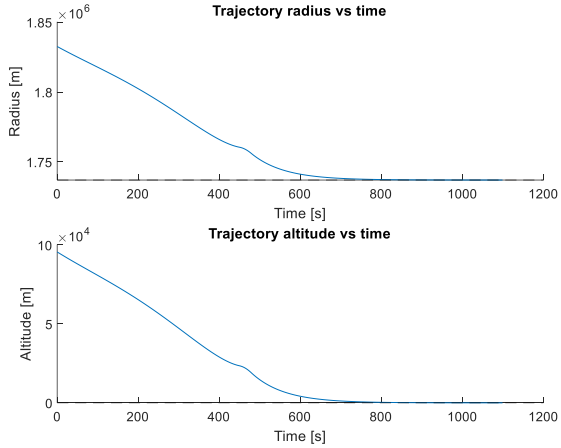

Fig. 6 PD radius and altitude descent.

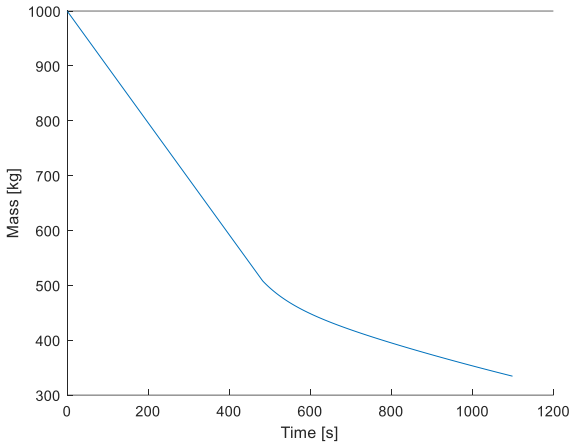

Fig. 7 PD mass depletion.

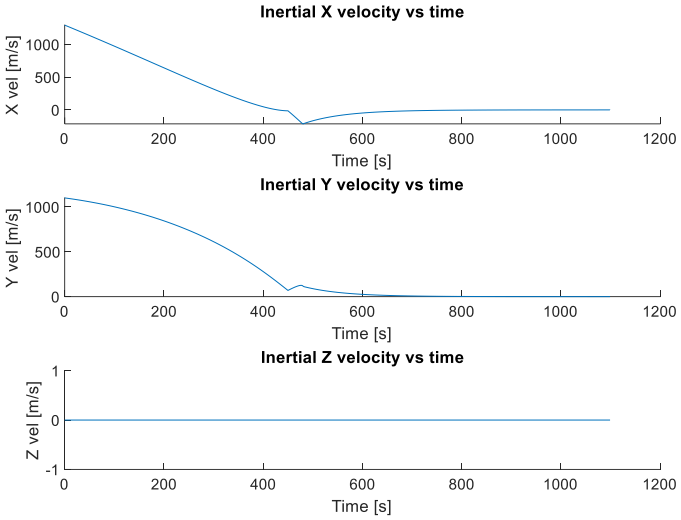

Fig. 8 PD descent velocity components.

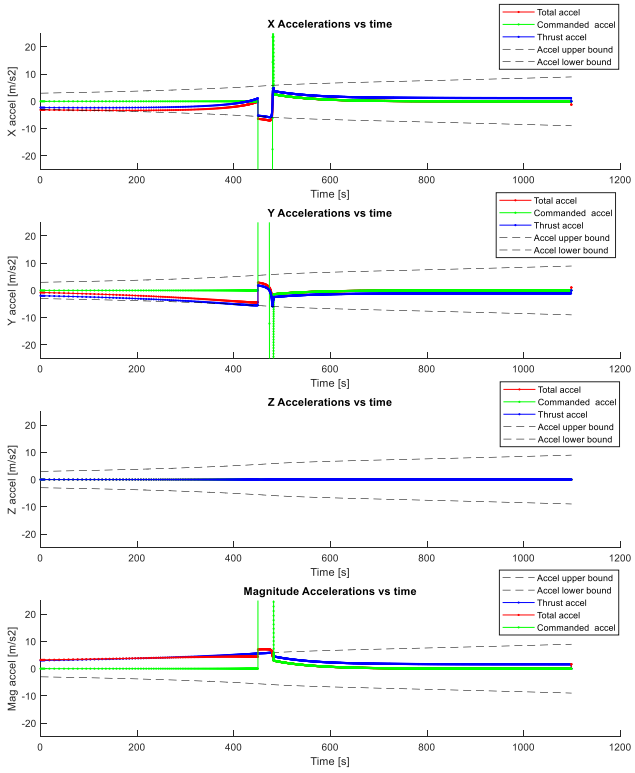

Fig. 9 PD descent accelerations components.

The descent took approximately 1099 s, with a landing speed of 1.279 m/s, and a landing position approximately 0.1048 m from the target. The final vehicle mass is 334.6 kg.

VI. Guidance Simulation: ZEM/ZEV I

The ZEM/ZEV approach is identical to the PD approach for the first 450 s, then the ZEM/ZEV equations defined in Eqs. (21–23) are implemented. The ZEM/ZEV formulation is taken from a waypoint ZEM/ZEV feedback algorithm [7].

$$\boldsymbol{a}_{cmd} = \frac{6}{t_{go}} \cdot \boldsymbol{ZEM} + \frac{2}{t_{go}} \cdot \boldsymbol{ZEV} \tag{21}$$

$$\boldsymbol{ZEM} = \boldsymbol{r}_{X,target} - (\boldsymbol{r}_X + \boldsymbol{v}_X \cdot t_{go} + \frac{1}{2} {t_{go}}^2 \cdot \boldsymbol{g}_X) \tag{22}$$

$$\boldsymbol{ZEV} = 0 - (\boldsymbol{v}_X + t_{go} \cdot \boldsymbol{g}_X) \tag{23}$$

Time to go is selected from the maximum value of Eqs. (24) or (26), or 0.5 s, to prevent ZEM/ZEV from computing a time to go below zero and reducing the chance for the acceleration commands to induce a prolonged low altitude hover that results in the simulated vehicle running out of propellant. The final ZEM/ZEV guidance simulation in section VII uses a polynomial-based time-to-go estimation.

$$t_{go} = \sqrt{\frac{2 \cdot r_{X,toTarget}}{a_{max}}} \tag{24}$$

$$\boldsymbol{r}_{X,toTarget} = \boldsymbol{r}_{X,target} - \boldsymbol{r}_X \tag{25}$$

$$t_{go} = \frac{v_X}{a_{max}} \tag{26}$$

The result is a descent described in Figs. 10 through 15.

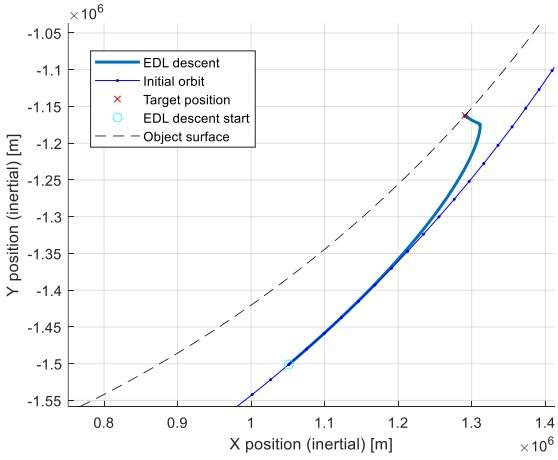

Fig. 10 ZEM/ZEV I EDL descent trajectory.

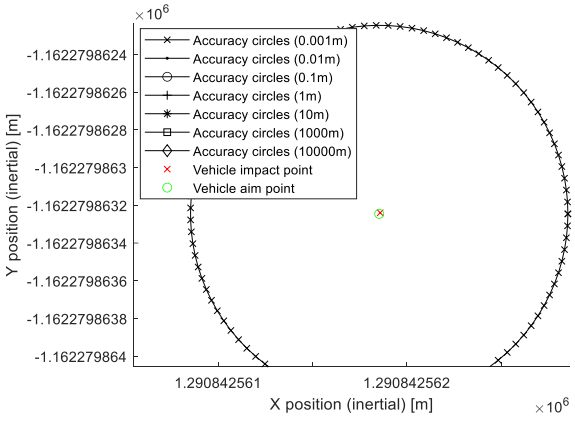

Fig. 11 ZEM/ZEV I landing accuracy.

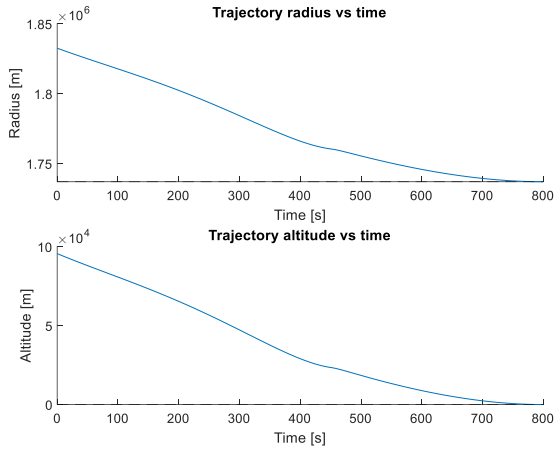

Fig. 12 ZEM/ZEV I radius and altitude descent.

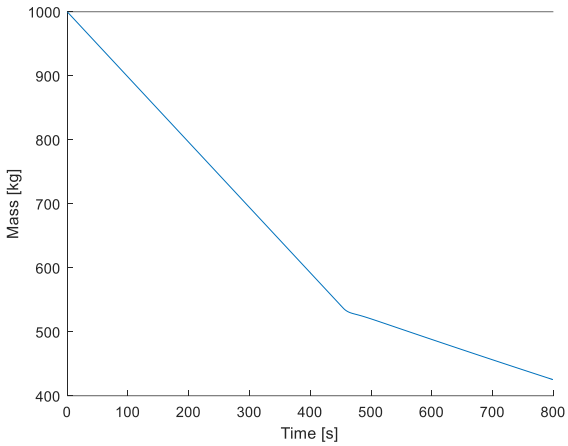

Fig. 13 ZEM/ZEV I mass depletion.

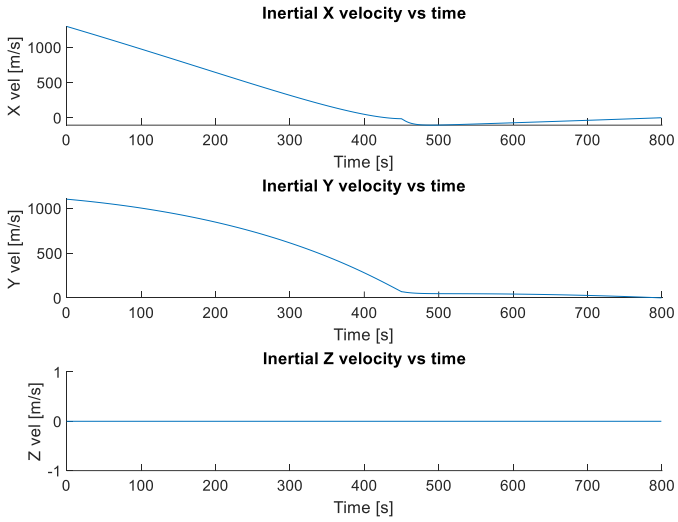

Fig. 14 ZEM/ZEV I descent velocity components.

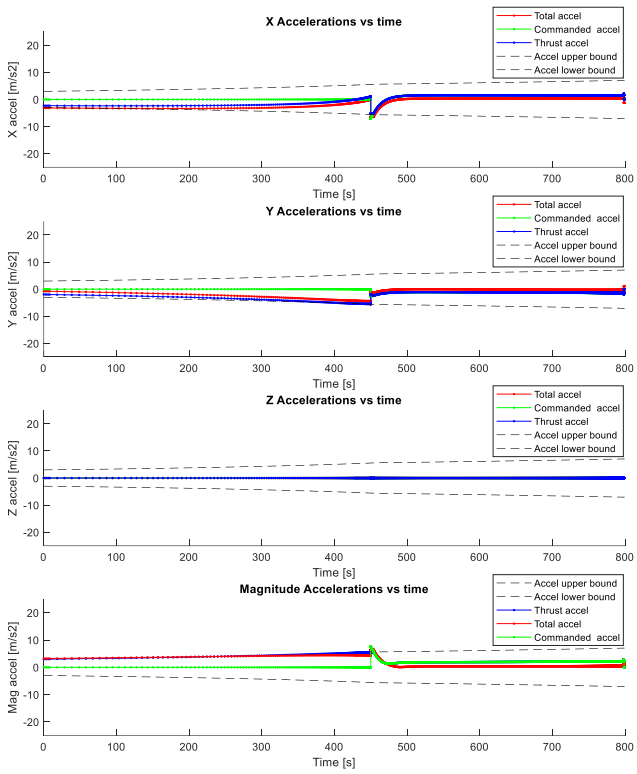

Fig. 15 ZEM/ZEV I descent acceleration components.

The descent took approximately 799.2 s, with a landing speed of 1.331 m/s, and a landing position approximately 0.000008072 m from the target. The final mass is 425.5 kg.

VII. Guidance Simulation: ZEM/ZEV II

The overall ZEM/ZEV II architecture is the same as that of ZEM/ZEV I; however, the time-to-go estimation used for t_{go} is now computed primarily by the D'Souza guidance time-estimation polynomial equation. If this solver fails, by producing all negative numbers or imaginary solutions, the position-based time estimate from Eq. (24) is used. This reversion was observed occasionally in the Monte Carlo runs for perhaps one or two timesteps and is not seen in the nominal case. The equations for the D'Souza guidance polynomial are Eqs. (27–30) [8]:

$$t_{go}{}^4 + a \cdot t_{go}{}^2 + b \cdot t_{go} + c = 0 \tag{27}$$

$$a = -\frac{2(\boldsymbol{v}_X \cdot \boldsymbol{v}_X)}{\Gamma + \frac{g_X{}^2}{2}} \tag{28}$$

$$b = -\frac{12(\boldsymbol{v}_X \cdot \boldsymbol{r}_X)}{\Gamma + \frac{g_X{}^2}{2}} \tag{29}$$

$$c = -\frac{18(\boldsymbol{r}_X \cdot \boldsymbol{r}_X)}{\Gamma + \frac{g_X{}^2}{2}} \tag{30}$$

In Eqs. (28–30), Γ can be set to a large positive number for minimum landing time or set to zero for minimum acceleration and maximum propellant efficiency. In this simulation, Γ is set to 70. As with the other ZEM/ZEV and PD guidance methods, when the altitude reaches 0.5 m all thrust commands are nulled. The result is a descent described in Figs. 16 through 21.

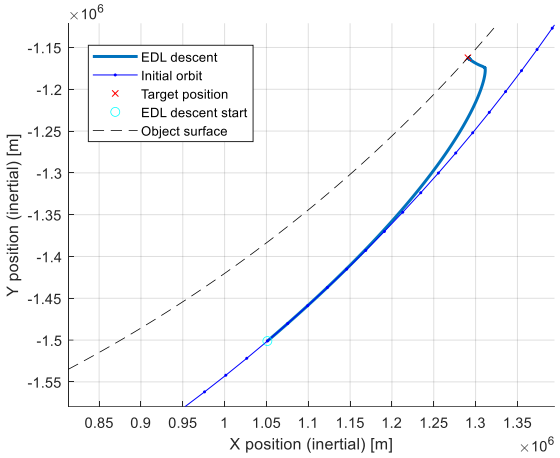

Fig. 16 ZEM/ZEV II EDL descent trajectory.

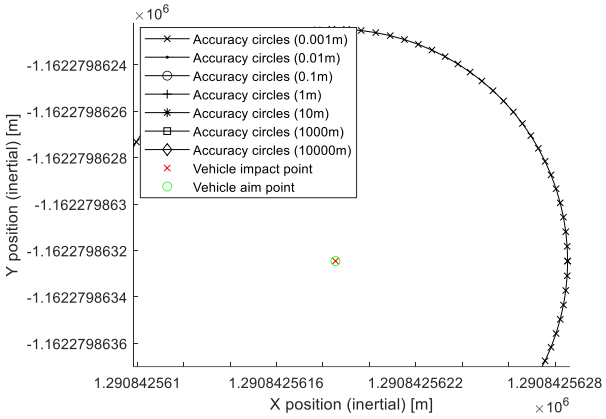

Fig. 17 ZEM/ZEV II landing accuracy.

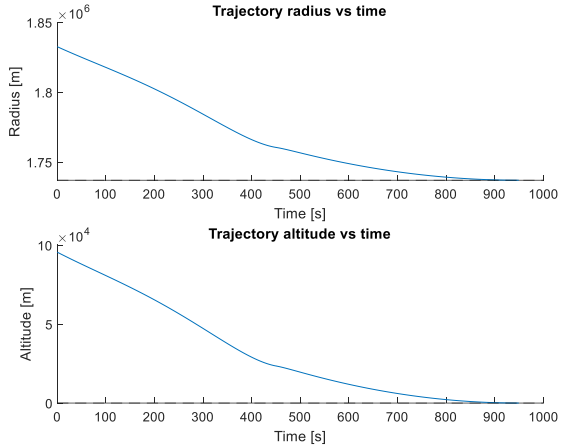

Fig. 18 ZEM/ZEV II radius and altitude descent.

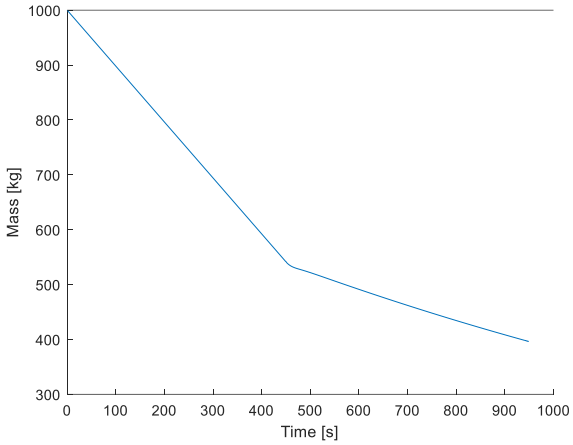

Fig. 19 ZEM/ZEV II mass depletion.

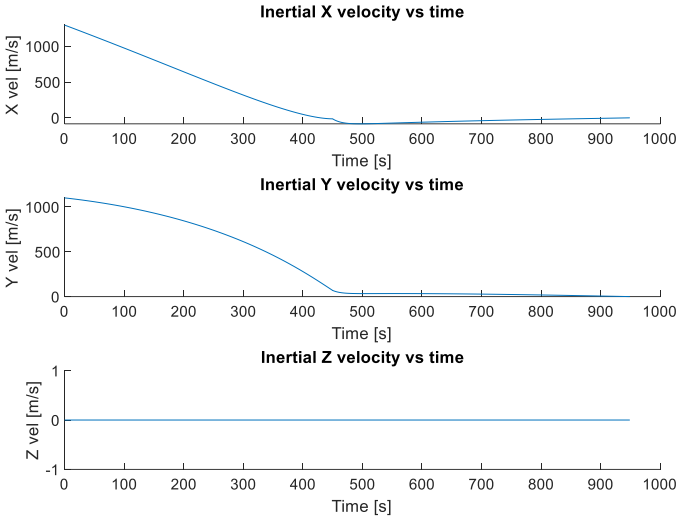

Fig. 20 ZEM/ZEV II descent velocity components.

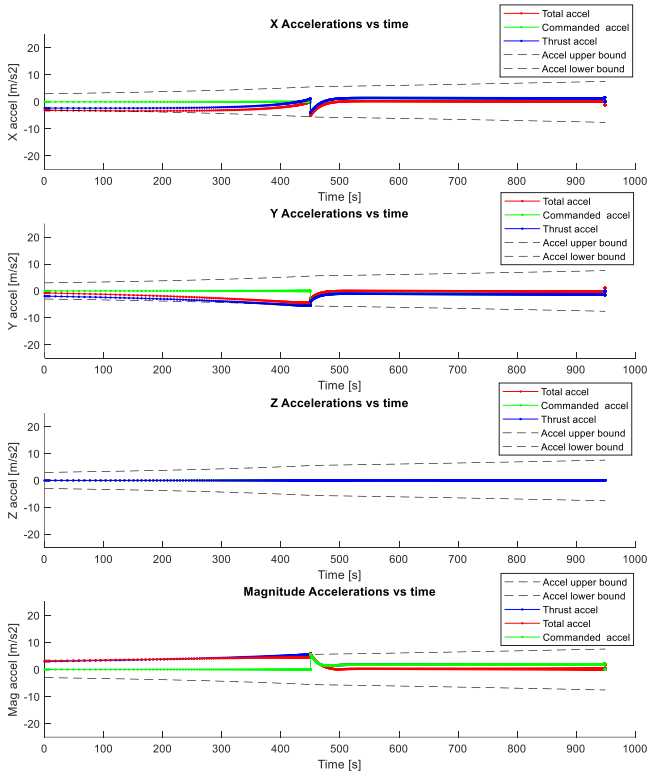

Fig. 21 ZEM/ZEV II descent acceleration components.

The descent took approximately 949.1 s, with a landing speed of 1.330 m/s and a landing position approximately 0.00000006957 m from the target. The final mass is 396.4 kg.

VIII. Comparison of Nominal Results

The key terminal results are reported in Table 4.

Table 4 Summary of nominal simulations

Guidance Type	Miss Magnitude [m]	Impact Speed [m/s]	Flight Time [s]	Final Mass [kg]
PD	0.1048	1.279	1099	334.6
ZEM/ZEV I	0.000008072	1.331	799.2	425.5
ZEM/ZEV II	0.00000006957	1.330	949.1	396.4

Figures 22 through 24 depict the difference in the PD and ZEM/ZEV profiles compared to an unguided descent. The unguided descent misses the target point by approximately 10 km.

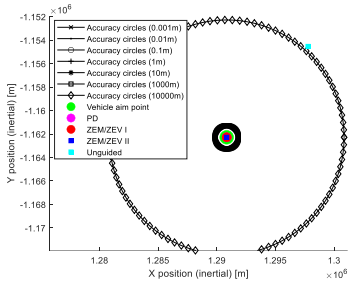

Fig. 22 Landing accuracy large view.

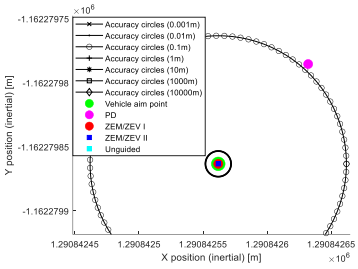

Fig. 23 Landing accuracy medium view.

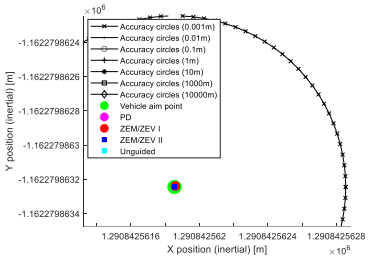

Fig. 24 Landing accuracy small view.

As seen in Figs. 22 through 24, the unguided trajectory is well outside the 1 km and smaller error circles, impacting approximately on the 10 km circle. The PD guidance scheme is a few orders of magnitude higher than those of the ZEM/ZEV I and II schemes. The two ZEM/ZEV schemes are also two magnitudes apart in accuracy; however, both are well within the 0.001 m accuracy circle and approaching the tolerance limit set for the ODE45 solver, which is 1e-9 in this simulation.

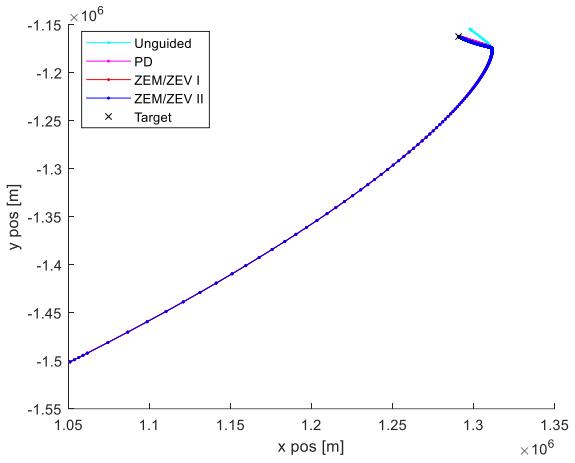

Fig. 25 EDL descent trajectory x-y plane view.

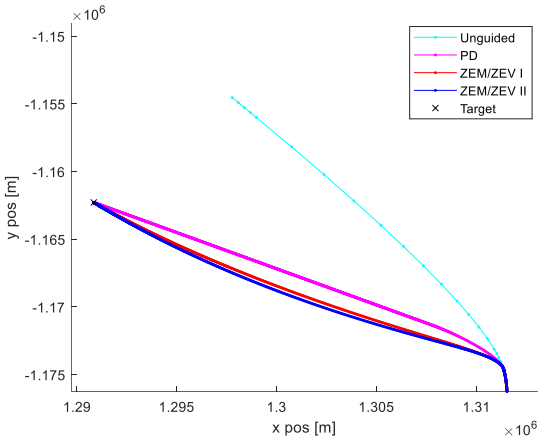

Fig. 26 EDL descent trajectory x-y plane zoomed view.

Figures 25 and 26 depict the planar trajectory of the vehicle for the different guidance schemes. Both ZEM/ZEV schemes bend inward while the no-guidance scheme follows the outward free-fall trajectory. The PD descent follows a relatively straight path to the target.

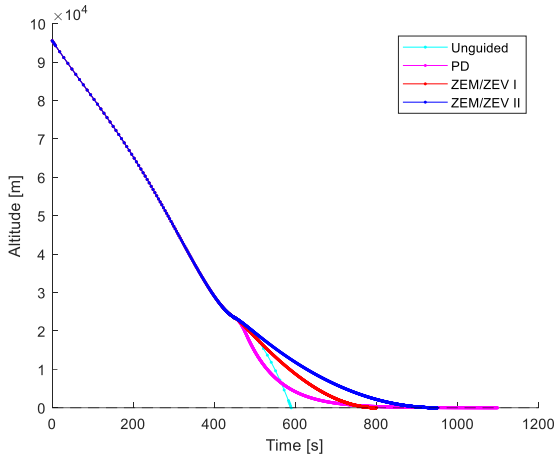

Fig. 27 EDL descent altitude.

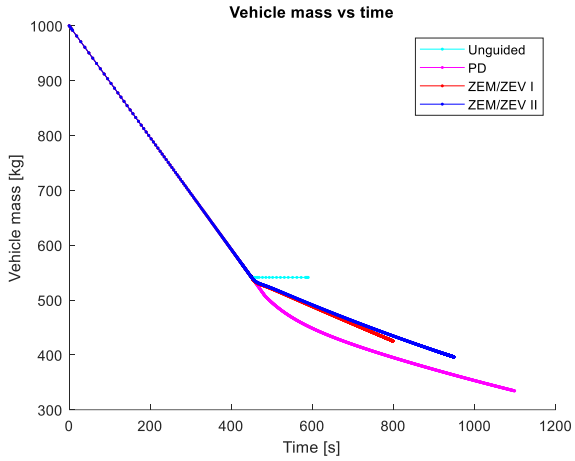

Fig. 28 EDL mass depletion over time.

Figure 27 shows the different guidance schemes and their altitude descent profiles. Aside from the unguided descent, the PD descent drops the quickest, even initially outpacing the free-fall only unguided descent. Both ZEM/ZEV descents follow less curved descents with the polynomial time-to-go estimator of ZEM/ZEV II taking longer than that of ZEM/ZEV I. In Fig. 28, the propellant consumption of each guidance scheme is visible. As expected, the unguided trajectory with no thrust after the initial burn uses the least propellant but impacts at high speed. The most efficient method is ZEM/ZEV I followed by ZEM/ZEV II and then PD. The differences in the time-to-go estimator for ZEM/ZEV I and II are shown in Fig. 29.

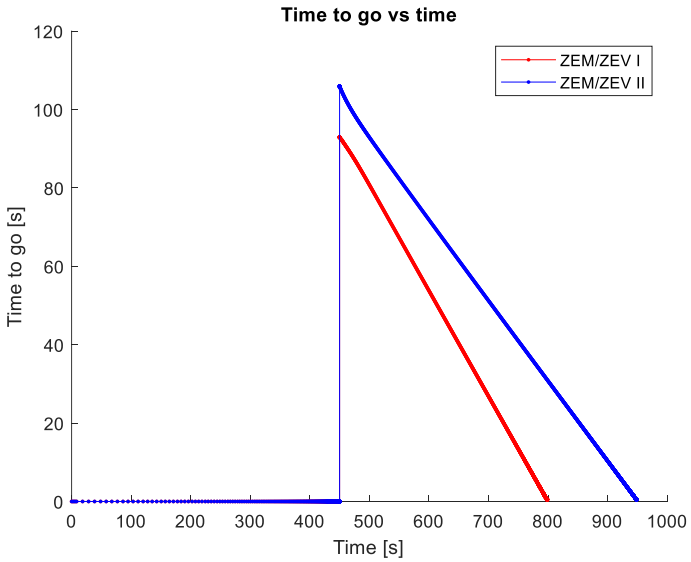

Fig. 29 ZEM/ZEV I/II time to go.

When guidance begins, the time-to-go values for both ZEM/ZEV guidance schemes are immediately initialized differently. Throughout, ZEM/ZEV II maintains a longer time to go relative to that of ZEM/ZEV I, and the slope is different for each, with the ZEM/ZEV I time to go decreasing at a faster rate than that of ZEM/ZEV II.

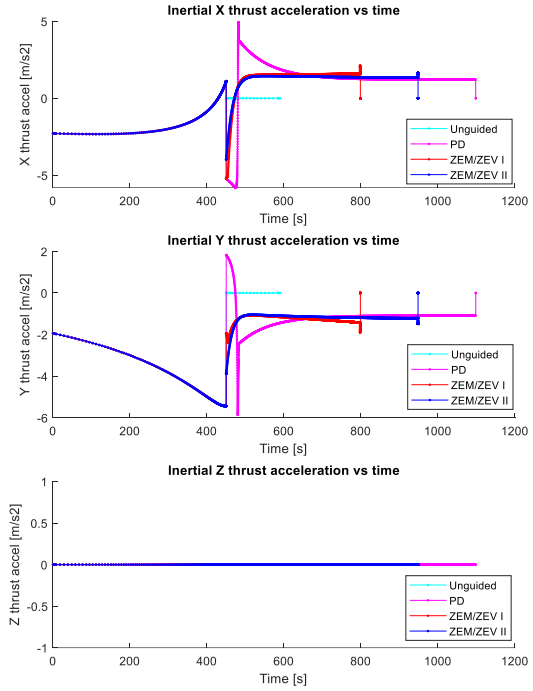

Fig. 30 EDL commanded thrust accelerations.

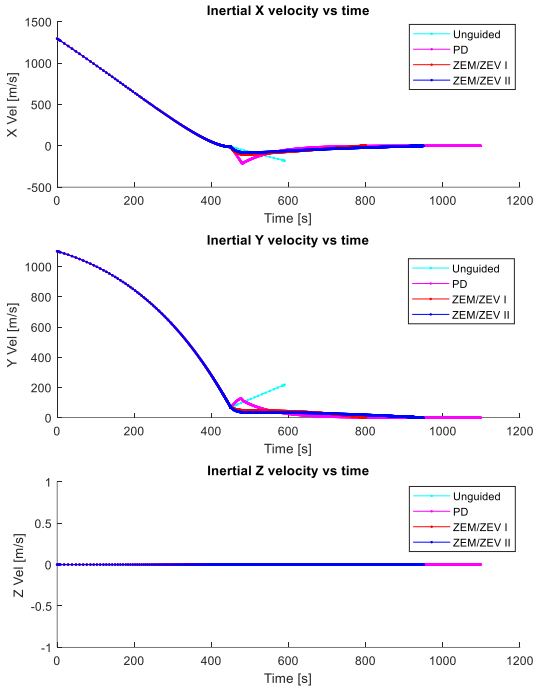

Fig. 31 EDL velocity components.

The commanded thrust accelerations in Fig. 30 provide the best insight into the different guidance schemes. They also provide some context for the velocity changes seen in Fig. 31. The PD guidance saturates the max thrust for the longest and has the highest desired acceleration demands. Additionally, it is the only guidance scheme that commands positive y thrust at the handover to the guidance schemes after the timed burn. ZEM/ZEV II has a lower max acceleration command than that of ZEM/ZEV I; however, both respond in the same directions at the same time, which is as expected.

The positive y acceleration commanded by the PD guidance is seen as a large velocity increase in Fig. 31. This erratic acceleration commanded by the PD guidance scheme adds to the propellant cost because this velocity has to be cancelled again. The erratic behavior also explains, in part, why the PD guidance takes longer and uses more propellant than the other methods.

Before turning to the Monte Carlo results, it is important to discuss the high accuracy of all the guidance methods, particularly the ZEM/ZEV I and II results. The simulation used in this study is operating under near ideal conditions. Every step in the ODE45 solver, regardless of how short the step may be, calls the guidance functions and returns a thrust command; the thrust is computed and delivered immediately; and orientation is not considered. Any throttle constraints on the engine are also not considered. In effect, if this were a real descent vehicle, which is impossible, it would have infinitely fast and accurate sensors, and the capability to provide 0 to 3000 N of thrust in any direction immediately. Lastly, the dynamics function feeds the guidance methods with a perfect gravity vector, which enables very high-fidelity guidance for the ZEM/ZEV schemes.

IX. Comparison of Monte Carlo Results

The reader may have noticed the z component of commands is silent in the nominal guidance simulations. This is because the orbit has no inclination and the target is directly below this equatorial orbit. The purpose of the Monte Carlo simulation is to add inclination and vary the large timed burn and engine parameters to understand at a high level the robustness of each guidance scheme. The Monte Carlo variables are shown in Table 5 with the average (nominal case) value and the selected standard deviation.

Table 5 Monte Carlo Variables

Parameter	Nominal Value	Standard Deviation
Vehicle mass [kg]	1000	3.3
Engine thrust [N]	3000	9.9
Engine IPS [s]	300	1.5
Timed burn length [s]	450	3.7
True anomaly at timed burn start [deg]	305	1
Periapsis altitude [m]	10000	33
Apoapsis altitude [m]	500000	8125
Inclination angle [deg]	0	1

For reference, Fig. 32 shows a 3D plot of the no-guidance descent, including the initial orbits, burn start, and end times. The Monte Carlo simulation uses 100 runs with a set random seed value of 120.

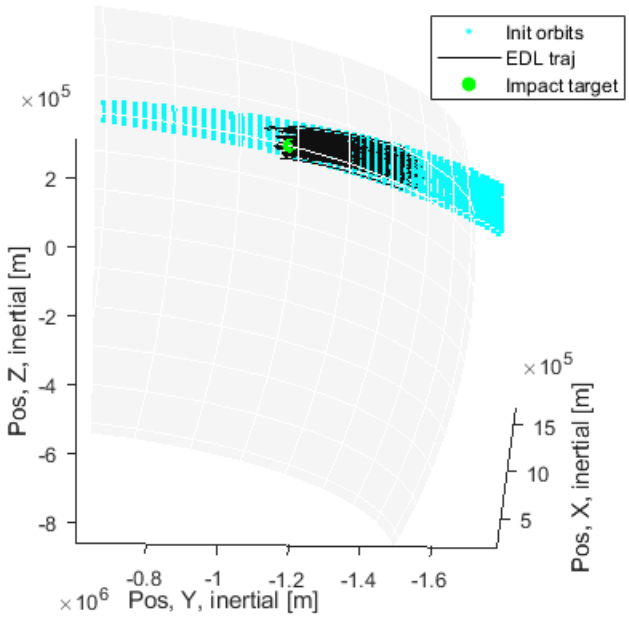

Fig. 32 3D unguided EDL descent case.

Figures 33 through 36 show 2D impact plots, including the miss distances of the different guidance schemes, and color coding for impact speeds.

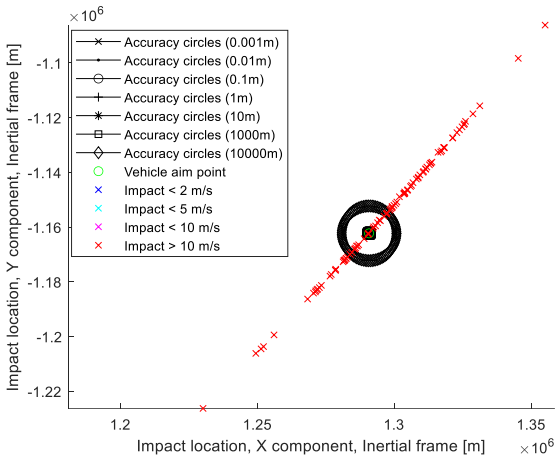

Fig. 33 Unguided landing accuracy.

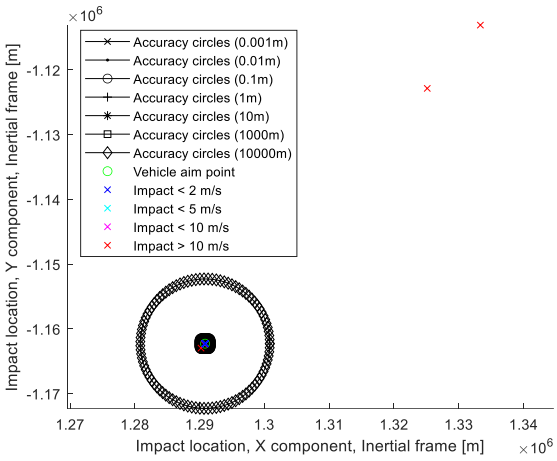

Fig. 34 PD landing accuracy.

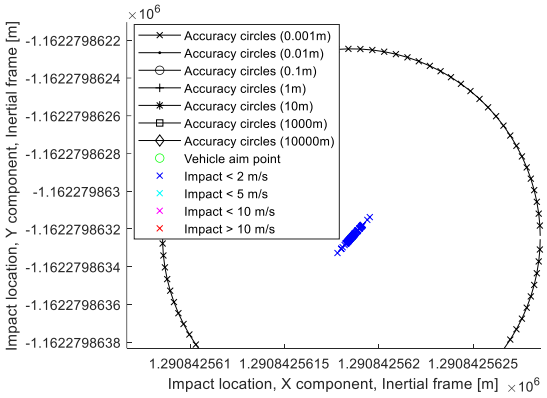

Fig. 35 ZEM/ZEV I landing accuracy.

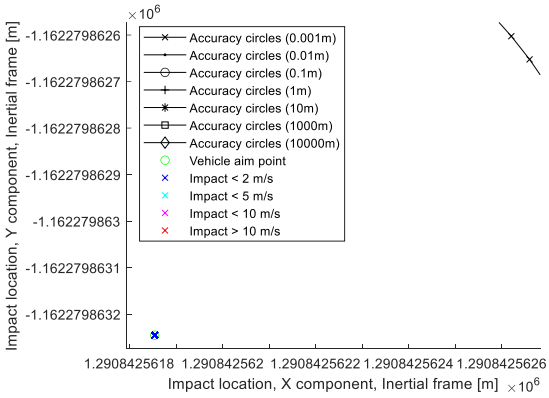

Fig. 36 ZEM/ZEV II landing accuracy.

The Monte Carlo variability can be seen in Fig. 32, where the timed burn ends and the descent sequence, the black line, takes over. The target is shown as the green dot and the initial orbits are the cyan points. In Fig. 33, it is clear that the variability has enormous spread on the unguided case, with miss distances well outside the 10 km accuracy circle as well as some lucky impacts within the accuracy circles, but well above a survivable landing speed. Figure 34 shows the PD guidance scheme with high variability and several large misses at high velocity contrasting with a large number within the accuracy circles at slow landing speeds. Figure 35 shows the ZEM/ZEV I scheme with very high accuracy and slow landing speeds. Figure 36 shows the ZEM/ZEV II scheme with even higher accuracy, to the point the impacts seemed to be stacked on top of each other at the same scale, coupled with similar slow landing speeds. Tables 6 through 9 provide summaries of the Monte Carlo results for the unguided, PD, ZEM/ZEV I, and ZEM/ZEV II cases.

Table 6 Results of the Monte Carlo miss distance

Guidance Scheme	Min Value [m]	Average Value [m]	Max Value [m]	Standard Deviation [m]
Unguided	267.4	25730	99660	19710
PD	0.004461	1189	65030	8300
ZEM/ZEV 1	0.0000007914	0.00003894	0.0001458	0.00002882
ZEM/ZEV 2	0.000000004622	0.0000001740	0.0000003267	0.00000008265

As shown in Table 6, the unguided scheme gets a lucky closest miss of 267.4 m while averaging about 25 km and maxing out at 99 km. The PD guidance scheme has a very high variability with a minimum miss of 0.004461 m and a maximum miss of around 65 km. The ZEM/ZEV schemes have very low miss distances and deviations, demonstrating their robustness to the current regime of Monte Carlo variable spread.

Table 7 Results of the Monte Carlo impact speed

Guidance Scheme	Min Value [m/s]	Average Value [m/s]	Max Value [m/s]	Standard Deviation [m/s]
Unguided	252.4	283.8	323.6	14.96
PD	1.279	14.58	648.4	86.85
ZEM/ZEV 1	1.331	1.331	1.331	0.000008047
ZEM/ZEV 2	1.330	1.331	1.331	0.00000005330

The key to understanding the high PD miss distances can be seen in the velocity data in Table 7, which shows the maximum impact velocity is almost twice as great for the PD guidance scheme as for the unguided impact. These data indicate there are conditions inside this Monte Carlo regime that the PD guidance cannot correctly guide to and, as a result, will instead accelerate towards the surface. As seen with the miss distances, the ZEM/ZEV schemes have low impact speeds and deviations, while the lowest speed occurs with PD guidance: that speed is only around 0.05 m/s slower than that of the ZEM/ZEV schemes.

Table 8 Results of the Monte Carlo descent time

Guidance Scheme	Min Value [s]	Average Value [s]	Max Value [s]	Standard Deviation [s]
Unguided	552.2	591.2	625.3	14.57
PD	552.4	1112	1169	89.43
ZEM/ZEV 1	794.4	862.0	1031	46.74
ZEM/ZEV 2	942.7	1045	1317	73.62

As shown in Table 8, the ZEM/ZEV II scheme has the longest descent time and, unlike the results for the miss distance and impact speed, has a higher deviation for descent time than that achieved by the ZEM/ZEV I guidance scheme. This difference could be the result of the time-to-go estimator interpreting the true time to go more accurately across the regime or that the coefficient Γ is not aggressive enough to encourage acceleration to force a quicker landing across the Monte Carlo regime.

Table 9 Results of the Monte Carlo vehicle final mass

Guidance Scheme	Min Value [kg]	Average Value [kg]	Max Value [kg]	Standard Deviation [kg]
Unguided	530.0	541.2	555.5	5.538
PD	300.0	315.2	439.3	20.56
ZEM/ZEV 1	348.5	401.6	432.1	16.60
ZEM/ZEV 2	308.0	369.1	401.3	19.18

Again, a trend in vehicle mass, similar to that of the descent time, can be seen in Table 9 for the two ZEM/ZEV schemes, with ZEM/ZEV II having a greater propellant consumption and deviation than ZEM/ZEV I. However, PD guidance consumes the most propellant and even hits the 300 kg threshold, meaning the simulation triggered the out-of-propellant flag and disabled all thrust.

Figures 37 through 39 support the tables above and provide further insight into the guidance behaviors.

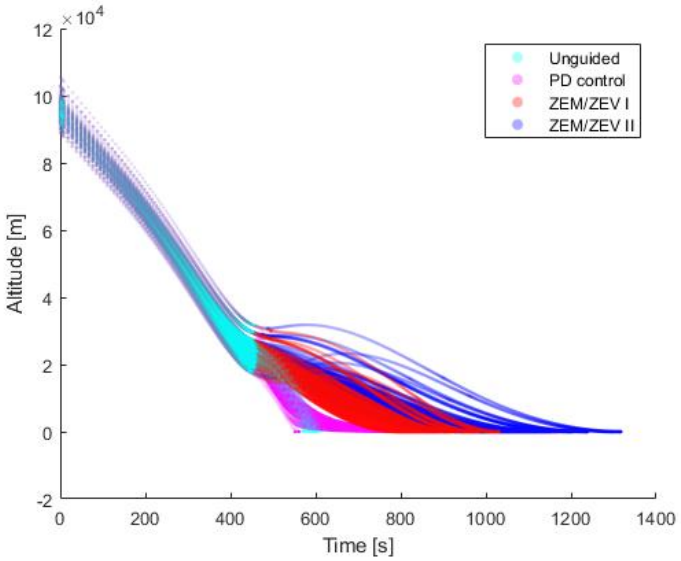

Fig. 37 Monte Carlo altitude plot of EDL guidance schemes.

As shown in Fig. 37, the behavior seen in the tabulated results matches that of the plotted data. An interesting result is the handful of PD runs that impact before the unguided descent. These results can also be observed in Fig. 38, which shows unnecessary velocity gains and losses during PD guidance, again indicating non-ideal acceleration guidance commands. It is also clear again from the slope of the velocity changes that significantly more magnitude in commanded acceleration was used across the runs for the PD guidance, which was also seen in the nominal PD run case. This high commanded acceleration is a result of the high gain, but a high gain is necessary to force the controller to reduce the speed expediently.

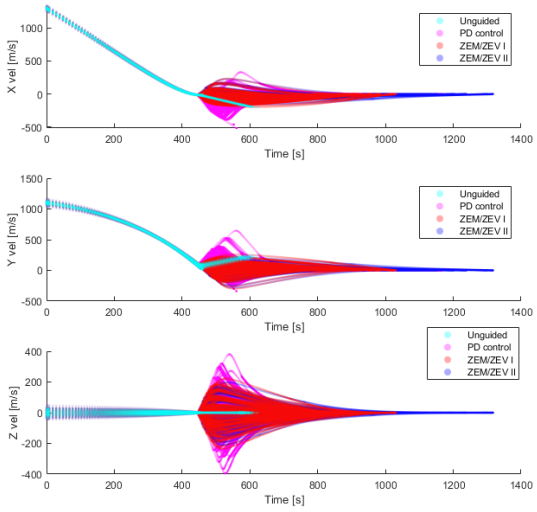

Fig. 38 Monte Carlo velocity component plot of EDL guidance schemes.

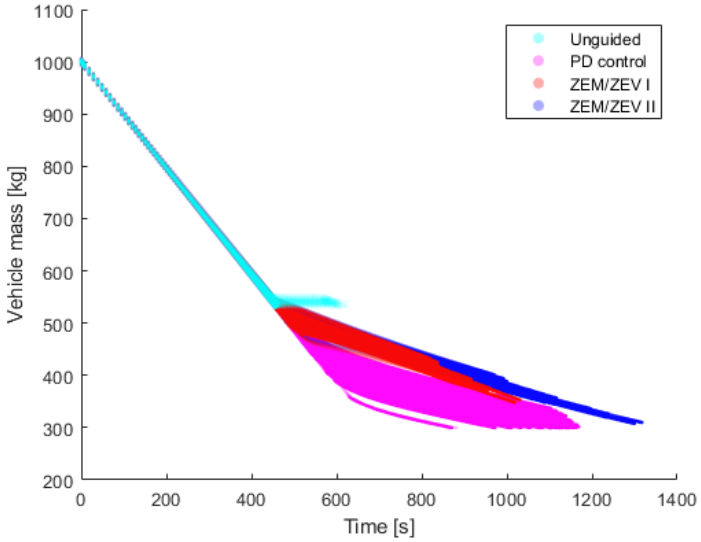

Fig. 39 Monte Carlo mass plot of EDL guidance schemes.

Figure 39 shows the mass of the vehicle, indicating that several of the PD simulations run out of propellant or almost run out of propellant and stop being able to thrust after hitting the 300 kg mark. The scheme with the greatest propellant margin is the ZEM/ZEV I guidance scheme. In this ideal scenario, the ability to save approximately 30 kg of propellant, decrease time spent in descent, and only reduce the landing accuracy from 10e-7 to 10e-5 is an efficient trade-off, and it would seem that ZEM/ZEV I would be the best choice. However, when a true payload is modeled with errors and uncertainties, the two orders of difference in accuracy magnitude between ZEM/ZEV I and ZEM/ZEV II may become critical to guaranteeing a pinpoint landing, and ZEM/ZEV II may emerge as the prudent choice.

References

[1] Sakai, S.-I., Japan Aerospace Exploration Agency, "Smart Lander for Investigating Moon (SLIM) Project Review Press Briefing," Institute of Space and Astronautical Science, Dec. 26, 2024. URL: https://www.isas.jaxa.jp/en/topics/files/SLIM-press-briefing-20241226.pdf [retrieved: 1 April 2026].

[2] Berger, E., "For Lunar Cargo Delivery, NASA Accepts Risk in Return for Low Prices," *Ars Technica*, May 3, 2021, URL: https://arstechnica.com/science/2021/05/for-lunar-cargo-delivery-nasa-accepts-risk-in-return-for-low-prices/ [retrieved: 1 April 2026].

[3] Firefly Aerospace, "Blue Ghost Mission 1 Component Graphic," January 14, 2025, URL: http://fireflyspace.com/wp-content/uploads/2025/01/BGM1-Component-Graphic-vJan14-2025a.png [retrieved: 1 April 2026].

[4] Foust, J., "Firefly's Blue Ghost 1 Lands on the Moon," *SpaceNews*, March 2, 2025, URL: https://spacenews.com/fireflys-blue-ghost-1-lands-on-the-moon/ [retrieved: 1 April 2026].

[5] Curtis, H. D., *Orbital Mechanics for Engineering Students*, 3rd ed., Butterworth-Heinemann, Oxford, UK, 2014, Chaps. 2, 4, 6.

[6] Nise, N. S., *Control Systems Engineering*, 8th ed., Wiley, Hoboken, NJ, 2019, Chap. 9.

[7] Guo, Y., Hawkins, M., and Wie, B., "Waypoint-Optimized Zero-Effort-Miss/Zero-Effort-Velocity Feedback Guidance for Mars Landing," *Journal of Guidance, Control, and Dynamics*, Vol. 36, No. 3, May–June 2013, pp. 799–809. doi: 10.2514/1.58098

[8] D'Souza, C. N., "An Optimal Guidance Law for Planetary Landing," AIAA Paper AIAA-97-3709, Aug. 1997. doi: 10.2514/6.1997-3709.